Journal of Inorganic Biochemistry 264 (2025) 112809

Contents lists available at ScienceDirect

Journal of Inorganic Biochemistry

journal homepage: www.elsevier.com/locate/jinorgbio

Reinvestigation of the mechanism of dioxygen activation at a Mn^{II}(cyclam) center

Tarali Devi [a,b,*], Stefan Mebs [c], Dibya Jyoti Barman [b], Amanda Opis-Basilio [b], Michael Haumann [c], Kallol Ray [b,*]

[a] Indian Institute of Technology Hyderabad, Telangana 502284, India
[b] Institut für Chemie, Humboldt-Universität zu Berlin, Brook-Taylor-Straße 2, 12489 Berlin, Germany
[c] Department of Physics, Freie Universität Berlin, Arnimallee 14, 14195 Berlin, Germany

ARTICLE INFO

Keywords:
O_2 activation
Bis(μ-oxo) manganese dimer
Inverse kinetic isotope effect
High-valent manganese
Kinetic studies
Density functional theory

ABSTRACT

This study deals with the unprecedented reactivity of a [(cyclam)$Mn^{II}(OTf)_2$] (**3**-*cis*; OTf = $CF_3SO_3^-$) with O_2, which, depending on the presence or absence of a hydrogen atom donor like 1-hydroxy-2,2,6,6-tetramethylpiperidine (TEMPO-H), selectively generates di-μ-oxo Mn(III)Mn(IV) (**1**) or Mn_2^{IV} (**2**) complexes, respectively. Both dimers have been characterized by different techniques including single-crystal X-ray diffraction, X-ray absorption spectroscopy, and electron paramagnetic resonance. Oxygenation reactions carried out with labeled $^{18}O_2$ and Resonance Raman spectroscopy unambiguously show that the oxygen atoms present in the $Mn^{IV}Mn^{III}$ dimer originate from O_2. Experimental evidences are provided for a novel method of dioxygen activation involving three Mn ions or two Mn ions and TEMPO-H to generate the bis(μ-oxo)dimanganese(IV) or bis(μ-oxo) dimanganese(III, IV) cores, respectively.

1. Introduction

Dioxygen (O_2) activation at transition metal centers is key to achieving various metabolic functions, which often require the controlled oxidation of organic substrates [1–4]. Oxidative transformations facilitated by metal-mediated dioxygen activation are also industrially relevant in the context of the efficient utilization of O_2 as the naturally abundant oxidant in oxidation reactions [5,6]. Great efforts in the last decades have focused on understanding the mechanism of dioxygen activation at biologically relevant iron and copper centers [7–11]. A consensus mechanistic hypotheses has been established, where O_2 is sequentially reduced to metal-superoxides and (hydro) peroxides, before being converted to high-valent metal-oxo cores. Although the metal–oxo intermediates have been generally considered as the reactive species responsible for oxygenation reactions [12,13], arguments are also emerging regarding the involvement of metal–superoxo, –peroxo, or – hydroperoxo species as the key oxidants in oxidation reactions [14–17]. A number of biomimetic iron- and copper superoxide, (hydro)peroxide, and oxide moieties have also been generated via mechanisms reminiscent of the dioxygen activation mechanisms in biology, which have provided vital insights into the prerequisites necessary for the design of efficient catalytic systems [14–17].

Notably, many biological processes also involve selective activation of oxygen at manganese [18], another cheap and abundant metal. However, knowledge of the factors that control dioxygen reactivity of manganese is presently very limited. A number of manganese-dioxygen or high valent manganese-oxo complexes have been reported over the years [4,18–21]; however, their generation, in most cases, involve the use of activated oxygen such as H_2O_2, iodosylbenzene (PhIO) or peracids as oxidizing agents. Direct reduction of oxygen at Mn(II) or Mn(III) centers has been reported only in rare cases, albeit in presence of externally added reducing agents [22–25], substrates containing C—H bonds, or redox non-innocent thiolate or semiquinonate donations. The observed non-reactivity of Mn(II) centers towards dioxygen, as reported in biomimetic studies, is also consistent with the Mn_2^{II} cofactor found in class 1b ribonucleotide reductase [26,27], which is proposed to be unreactive towards O_2 and requires a superoxide anion ($O_2^{\cdot-}$), generated by reduction of O_2 by a flavodoxin protein (flavodoxin hydroquinone, $NrdI_{hq}$), to assemble an oxo-bridged dimanganese(III,IV) species.

More relevant to the present study is the report from Brewer et al. [28,29], where the generation of an oxo-bridged dimanganese(III,IV)

* Corresponding authors at: Institut für Chemie, Humboldt-Universität zu Berlin, Brook-Taylor-Straße 2, 12489 Berlin, Germany.
E-mail addresses: taralidevi@chy.iith.ac.in (T. Devi), kallol.ray@chemie.hu-berlin.de (K. Ray).

https://doi.org/10.1016/j.jinorgbio.2024.112809
Received 15 September 2024; Received in revised form 19 November 2024; Accepted 7 December 2024
Available online 9 December 2024

species $[(cyclam)_2Mn_2O_2]^{3+}$ (**1**) was demonstrated upon aerial oxidation of an in situ generated $[Mn^{II}(cyclam)]^{2+}$ (cyclam = 1,4,8,11-tetraazacyclotetradecane, Fig. 1) complex in presence of water. Although Brewer et al. initially hypothesized water as the source of oxygen atoms in the Mn_2O_2 core, it was later contradicted by Nakamori et al. [31] in a subsequent study, where the generation of **1** was shown by exposing a dinuclear Mn^{II}-*p*-semiquinonato complex, $[Mn^{II,II}_2(cyclam)_2(\mu\text{-}SQ)_2]^{2+}$ (SQ = *p*-semiquinonato} to dioxygen in the absence of water. Based on this study Nakamori et al. proposed dioxygen as the source of oxygen atoms in the Mn_2O_2 core formed by the aerial oxidation of an $[Mn^{II}(cyclam)]^{2+}$ in presence of water, although the roles of water and the SQ ligand have not been explicitly defined in the reaction.

In the context of the controversy related to the conversion of $[(cyclam)Mn^{II}]^{2+}$ to **1** we report here the unprecedented reactivity of a well-defined $[(cyclam)Mn^{II}]^{2+}$ complex directly with O_2, in a pure N_4 coordination environment, in the absence of any external reductant or redox non-innocent ligands, to yield a high-valent bis(μ-oxo)dimanganese(IV) species, $[(cyclam)_2Mn_2O_2]^{4+}$ (**2**), which has been characterized by single crystal X-ray crystallography. Notably, when the same reaction is done in presence of a H-atom donor like 1-hydroxy-2,2,6,6-tetramethyl-piperidine (TEMPO-H), the corresponding one-electron reduced oxo-bridged dimanganese(III,IV) species **1** is formed. A full mechanism of O_2 activation, starting from $[(cyclam)Mn^{II}]^{2+}$ in presence and absence of TEMPO-H is proposed based on experimental and computational studies. In particular, we suggest a novel method of dioxygen activation by the involvement of either three Mn ions or two Mn ions and TEMPO-H in the transition state to generate the bis(μ-oxo) dimanganese(IV) or bis(μ-oxo) dimanganese(III, IV) cores, respectively.

2. Results and discussion

As previously reported, combination of the tetradentate cyclam ligand with $[Mn^{II}(OTf)_2]$ (OTf = $CF_3SO_3^-$) yields the manganese(II) cyclam complex, $[(cyclam)Mn^{II}(OTf)_2]$ (**3**-*cis*; Scheme 1 inset), in *cis*-V configuration of the macrocyclic ring (Fig. 1b) and two -*cis* triflates [30]. Characterization of **3**-*cis* was performed by scXRD, cyclic voltammetry (CV), electron paramagnetic resonance (EPR) and electrospray ionization mass spectrometry (ESI-MS) (**Supporting Information, SI**; **Fig. S1 & S2**), based on which a high-spin $S = 5/2$ Mn^{II} (d^5) center can be assigned, which is also supported by density functional theoretical calculations (**Table S1-S2a**).

When an acetonitrile (ACN) solution of **3**-*cis* was purged with dioxygen, the colourless solution slowly turned brown over a period of several hours, which then subsequently converted to a dark olive-green solution. Efforts to crystallize the olive-green species via the diethyl ether (Et_2O) diffusion method resulted in fine needle-shaped olive-green crystals of X-ray diffraction quality. The XRD structure (Fig. 2 and **Table S3**) revealed the presence of two Mn-centres bound to two O-atoms in a bis-μ-oxo fashion (**2**) and retention of the *cis*-V configuration with a centre of inversion in the unit cell. The presence of a symmetry element '*i*' in the crystal structure suggested both the Mn-centres to be chemically equivalent, which is also reflected in the Mn—O bond distances. An unoxidized $[(cyclam)Mn^{II}(OTf)_2]$ complex in the *trans*-III configuration (Fig. 1c) [30a] with two *trans*-OTf ligands also co-crystallized with the Mn_2O_2 unit. Based on the charge calculations, species **2** can be best formulated to be a Mn(IV, IV) bis-μ-oxo species. The Mn—O bond distances and Mn—Mn separation are found to be 1.826 (2) Å, 1.822 (2) Å and 2.730 (6) Å, respectively, which correlate with the reported bond distances of the rare examples of Mn(IV, IV) bis-μ-oxo complexes available in the literature (Table 1) [25,32–35]. DFT calculations predict an antiferromagnetic coupling between the two Mn (IV) states, providing a diamagnetic $S = 0$ ground state (**Table S2a**). The calculated metrical parameters are found to be in good agreement with the experiment (Table 1). The conversion of **3**-*cis* to **2** was found to be too slow (conversion in about 2 days at 25 °C) to be followed by UV–vis spectroscopy. The $Mn_2(\mu\text{-}O)_2$ unit of complex **2** is EPR silent, as expected; only the residual signal associated with the cocrystallized $[(cyclam)Mn^{II}(OTf)_2]$ moiety is observed in the EPR spectrum of **2**.

Interestingly, the dioxygen activation process by **3**-*cis* can be significantly facilitated by the presence of TEMPO-H (BDE of O-H = 70.6 $kcalmol^{-1}$) [36] in ACN at room temperature, and the reaction becomes amenable to be monitored by UV–vis spectroscopic techniques. The UV–vis spectral feature of the new species formed upon O_2 activation shows a sharp peak at 550 nm (ε = 318 M^{-1} cm^{-1}) and another band at 640 nm (ε = 288 M^{-1} cm^{-1}) with a shoulder at 375 nm (ε = 680 M^{-1} cm^{-1}) (Fig. 3a). The formation of this new species upon addition of TEMPO-H and O_2 to **3**-*cis* follows pseudo-first order kinetics (inset Fig. 3a, black trace). By varying the TEMPO-H concentration in a saturated ACN solution of O_2 the second order rate constants, k_H = 0.24 M^{-1} s^{-1} were determined. Interestingly by employing TEMPO-D the rate of reaction got faster (inset Fig. 3a, red trace) with an increased rate constant (k_D = 0.42 M^{-1} s^{-1}), thereby demonstrating an inverse kinetic isotope effect (KIE = 0.56) (Fig. 3b). The inverse KIE may demonstrate that the rate-determining O—O bond cleavage is coupled to Mn^{IV}O-H bond formation and not TEMPO-H bond cleavage, so that the more stable Mn^{IV}O-D interaction compared to Mn^{IV}O-H in the transition state will lower the activation barrier for O—O bond cleavage in presence of TEMPO-D (Scheme 1, **Path B**) [37,38]. The oxygenation of **3**-*cis* in presence of TEMPO-H is associated with the appearance of a $S = 1/2$ EPR signal corresponding to $TEMPO^{\bullet}$ (Fig. 4a) and another total spin $S_t = 1/2$ EPR signal centered at $g \approx 2$ with well-resolved 16 nuclear (^{55}Mn) hyperfine lines (Fig. 4b). The anisotropic g ($g_{\perp}^{eff} = 2.003$ $g_{\parallel}^{eff} = 2.005$) and hyperfine coupling constant, $|A|$ tensor ($|A(Mn_A)_{\perp,\parallel}|$ = [439, 204] MHz; $|A(Mn_B)_{\perp,\parallel}|$ = [225, 117] MHz) closely resemble the typical appearance of the numerous reported $Mn^{III}Mn^{IV}$ centers, both synthetic and biological [23,27,29,39]. The high stability of the generated species at room temperature led us to grow X-ray diffraction quality crystals by the Et_2O diffusion method, confirming the generation of a mixed-valent Mn(III, IV) bis-μ-oxo species (**1**) (Fig. 5; Tables 1 and **S4**). A trend of two short (Mn1-O2; Mn1-O1) and two long (Mn2-O2 and Mn2-O1) Mn—O distances is observed, consistent with the presence of Mn^{IV} and Mn^{III} centers, respectively, in **1**. The intermetallic distance of 2.731 (2) Å in **1** is, however, comparable to that observed for **2** (Table 1). The metrical parameters of **1** and **2** are well reproduced in the calculations

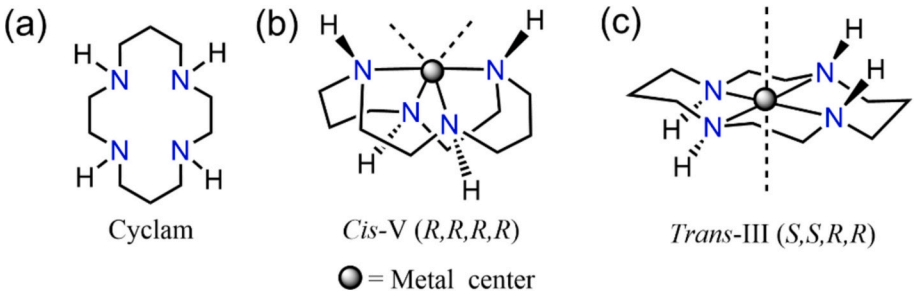

Fig. 1. (a) Chemical structure of cyclam ligand and (b), (c) the representative stereoisomers of the cyclam ligand relevant to this study.

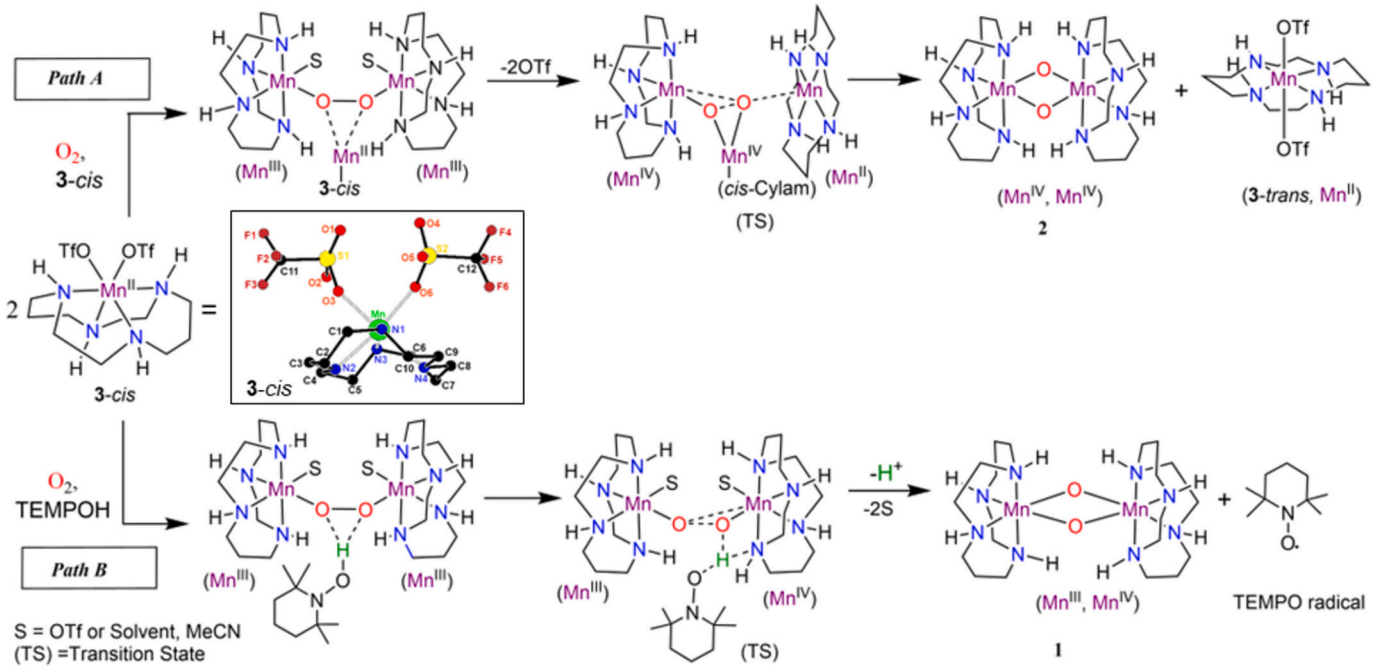

Scheme 1. Proposed reaction mechanism of O_2 activation by **3**-*cis* with and without TEMPO-H. The inset shows the atomic arrangement of **3**-*cis* in the solid state.

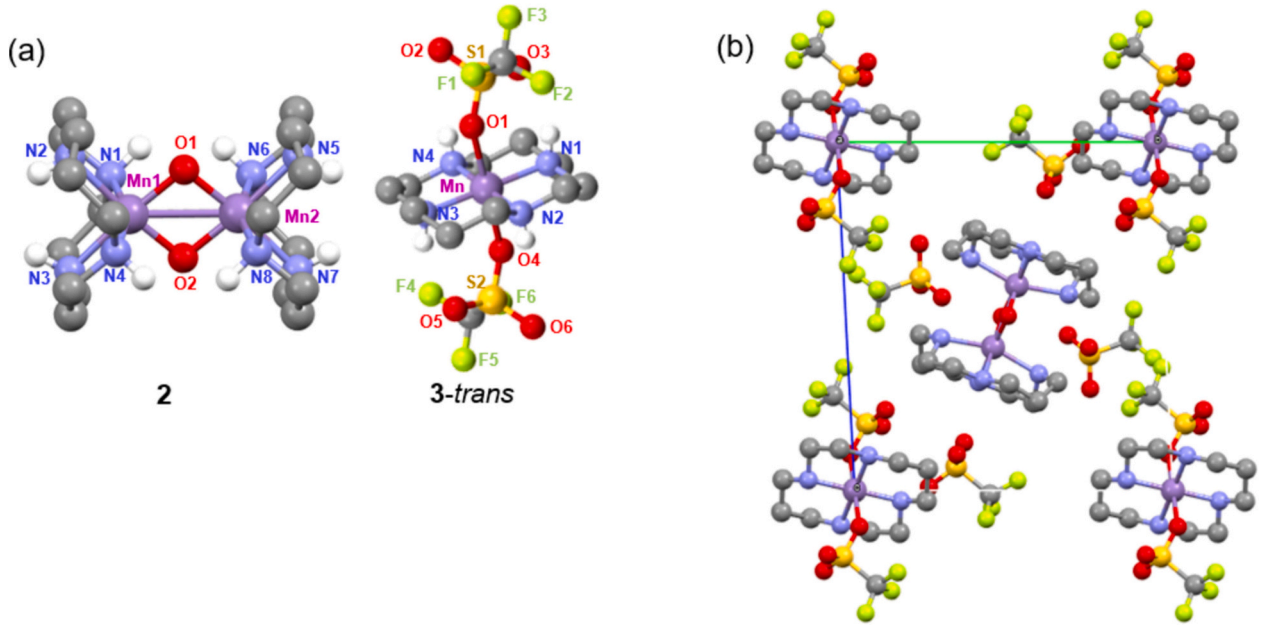

Fig. 2. (a) Single crystal XRD-determined molecular structure of **2** with co-crystallized **3-*trans***. Hydrogen atoms bonded with atoms other than nitrogen are removed for clarity. Selected bond distances of **2**: Mn1-O1 = 1.826 (2) Å, Mn1-O2 = 1.822 (2) Å, Mn2-O1 = 1.822 (2) Å, Mn2-O2 = 1.826 (2) Å and intermetallic separation: Mn1-Mn2 = 2.730 (6) Å. **Table S3** summarizes the crystallographic information. (b) Unit cell packing of the molecules in the crystal. Colour code: C: gray; N: blue; F: green; O: red; S: yellow, Mn: purple. (For interpretation of the references to colour in this figure legend, the reader is referred to the web version of this article.)

(**Table S2a-S2b**).

The resonance Raman spectrum of **1**, excited at 406 nm in ACN solution, exhibited isotope-sensitive bands at 608 cm^{-1} and 686 cm^{-1}, which shifted to 579 cm^{-1} and 656 cm^{-1}, respectively, upon ^{18}O labelling (Fig. 6) [39,40]. Based on DFT calculations (**Fig. S3**, **Table S2c**), the bands at 608 and 686 cm^{-1} are assigned as mixed valent Mn(III) − O and Mn(IV) − O stretching vibrations, which were calculated at 610 cm^{-1} and 712 cm^{-1}, respectively. The calculated $^{16}\Delta - {}^{18}\Delta$ values are also in good agreement with the experimental values of 29 cm^{-1} and 30 cm^{-1}.

Further structural information for **3**-*cis*, **1**, and **2** was obtained from X-ray absorption spectroscopy (XAS) studies carried out using both deep-frozen solid (powder) or liquid (ACN solution) samples. The K-edge energy close to 6546.5 eV of the X-ray absorption near edge structure (XANES) spectrum of **3**-*cis* in the solid state indicates Mn(II) [41]. Simulation analysis results of the extended X-ray absorption fine structure (EXAFS) spectrum of **3**-*cis* are compatible with the crystal structure, i.e., showing 4 N-ligands at Mn(II) (~2.25 Å) and suggesting two OTf ligands per manganese due to detection of respective Mn—O bonds and 2nd-sphere Mn—S distances (**Table S5, Fig. S4**). According to

Table 1
Comparison of selected bond lengths and intermetallic distances in different $Mn^{III}Mn^{IV}$ and $Mn^{IV}Mn^{IV}$ systems [34,39].

System	Bond length/intermetallic distance (Å)			Reference
	Mn1-Mn2	Mn1-O1 Mn1-O2	Mn2-O1 Mn2-O2	
$Mn^{III}Mn^{IV}$	2.731(2)	1.791(2)	1.856(2)	**1**, this work
	2.72 (EXAFS)	1.793(2) 1.79 (EXAFS)	1.858(2)	
	2.734	1.769	1.860	**1** (DFT), this work
	2.741(1)	1.786(5) 1.790(2)	1.855(2) 1.868(2)	[29]
	2.6483(8)	1.815(3) 1.812(3)	1.815(3) 1.812(3)	[23a]
	2.648(2)	1.787(5) 1.767(6)	1.835(6) 1.834(5)	[23a]
$Mn^{IV}Mn^{IV}$	2.730(6)	1.826(2)	1.822(2)	**2**, this work
	2.72 (EXAFS)	1.822(2) 1.79 (EXAFS)	1.826(2)	
	2.776	1.810	1.813	**2** (DFT), this work
	2.724(2)	1.794(4) 1.802(4)	–	[35]
	2.672(1)	1.812 (2) 1.810 (2)	–	[32]
	2.7821(16)	1.845(3) 1.809(3)	–	[25]

the shoulder in the XANES spectrum, the OTf ligands are in *cis* configuration. The overall structure with mainly Mn(II) was retained in ACN solution, however, the steeper XANES shape may suggest formation also of (some) **3**-*trans*, i.e., with a more centro-symmetric metal site vs. **3**-*cis*. Furthermore, the sizeable coordination number of long Mn—Mn distances (~3.6 Å) from EXAFS (**Fig. S5**) presumably shows small amounts of $Mn(III)_2$ species in solution. The K-edge energy (~6550 eV) of solid **2** matches with a mean Mn(III) oxidation level, in good agreement with one $Mn(IV)_2$ dimer per two Mn(II) monomers in the powder sample, similar to the crystal data. A similar K-edge energy for **2** in ACN solution indicates preservation of both the Mn(II) and Mn(IV, IV) species. The EXAFS analysis revealed about 0.5 coordination number of Mn-O/S distances in **2**, due to detachment of OTf ligands from a fraction of the metal centers, and an overall shortening of Mn-N/O by ca. 0.2 Å (relative to **3**-*cis*), in agreement with the formation of high-valent manganese species. In particular, the short Mn—O bonds (ca. 1.78 Å) are clearly indicative of μ-oxo bridges between the Mn(IV) ions. Sub-stoichiometric amounts of Mn—Mn distances were detected, with a metal separation of ~2.72 Å, which is similar to that obtained in the crystal structure analysis. The EXAFS results were similar for solid and solution samples of **2**, with only minor alterations in the interatomic distances, mainly in the 2nd coordination sphere, indicating stability of the $Mn(IV)_2$ species, also in the concentrated (5 mM) XAS solution samples (**Table S5, Fig. S4**). Notably, the results for **2** were reproduced in each of the two independent samples for XAS. The K-edge energy for **1** was in the middle between the Mn(II) and Mn(III) levels, in agreement with a mean Mn oxidation state of ca. 2.75 due to the Mn(III)Mn(IV) dimer of **1** and possibly residual Mn(II) of **3**-*cis* (due to incomplete conversion of **3**-*cis* to **1** in the concentrated XAS sample) and **3**-*trans* (below). A slightly steeper K-edge shape for **1** (i.e., the **3**-*cis* and **1** mixture) in solution vs. solid was presumably again explained by limited formation of **3**-*trans*. The respective EXAFS spectra were more dominated by the **3**-*cis* contributions compared to the samples of **2**, as also reflected in the smaller coordination numbers of short Mn—O bonds due to the bridging ligands and larger coordination numbers of manganese-OTf distances, as well as in the overall longer Mn-N/O bond lengths vs. **2**. The Mn—Mn distance of **1**, however, was still observed (~2.72 Å), although in lower amounts, and, in agreement with the crystal structure analysis, is indistinguishable from the distance of **2** (within the uncertainty limits of EXAFS simulation). In summary, the XAS data are in reasonable agreement with preservation of residual Mn(II) species and of Mn(IV)Mn(III) and $Mn(IV)_2$ dimers in solution samples, which are similar to the structures in powder (microcrystalline) material and in the single crystal structures.

3. Concluding remarks

The ligand architecture of metal-cyclam complexes has been previously demonstrated to play an important role in the dioxygen activation reaction. For example in $[(cyclam)Fe(CH_3CN)_2]^{2+}$ in *trans*-III configuration, the N—H bonds of the tetramethylcyclam ligand were found to aid the cleavage of the Fe^{III}–O–O–Fe^{III} bond homolytically by forming hydrogen bonds with the O_2 moiety, leading to a significantly lowered kinetic energy barrier for the high-valent oxoiron(IV) formation [10]. The O_2 activation ability is unique for the *trans*-III configuration of the cyclam macrocyclic ring; the corresponding iron complex with the *cis*-V configuration only performed reactions with hydrogen peroxide [42]. In the present study involving the manganese-cyclam complex, a different selectivity is observed. Whereas, $[(cyclam)Mn(OTf)_2]$ (**3**-*cis*) with *cis*-bound OTf ligands activate O_2 to form high-valent Mn(IV)-oxo centers, the corresponding complex **3**-*trans* with trans OTf ligands is stable against oxidation even in presence of highly oxidizing Mn(IV) centers. Furthermore, in contrast to *trans*-$[(cyclam)Fe(CH_3CN)_2]^{2+}$, the strength of the H-bonding interaction between the cyclam -NH groups and O_2 in the hypothetical manganese-dioxygen complex is presumably not strong enough to result in an efficient bimolecular activation of O_2. Indeed, only weak H-bonding interactions are observed in the DFT calculated

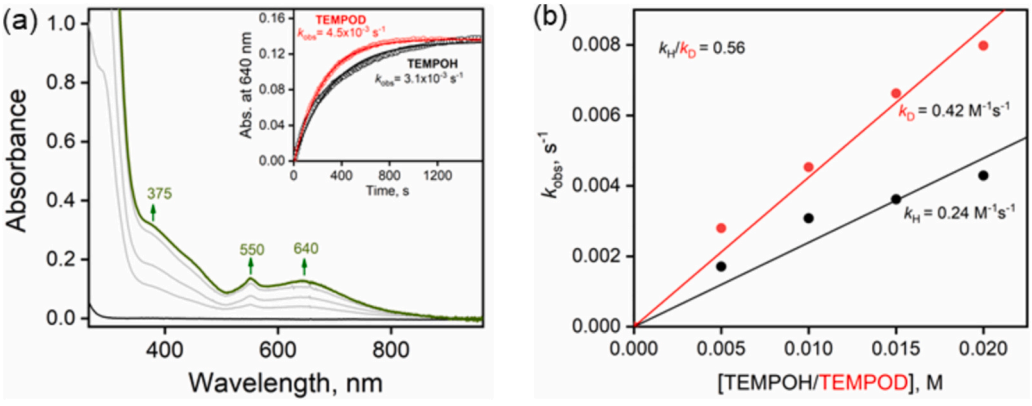

Fig. 3. (a) UV–vis spectral changes observed in the reaction of **3**-*cis* (0.5 mM) with O_2 in the presence of TEMPO-H (20 equiv.) in ACN at 298 K. The inset shows the time traces at 640 nm of the reaction with TEMPO-H (20 equiv., black) or TEMPO-D (20 equiv. red). (b) Plot of pseudo first-order rate constant (k_{obs}) vs. concentration of TEMPO-H (black plot) or TEMPO-D (red plot). (For interpretation of the references to colour in this figure legend, the reader is referred to the web version of this article.)

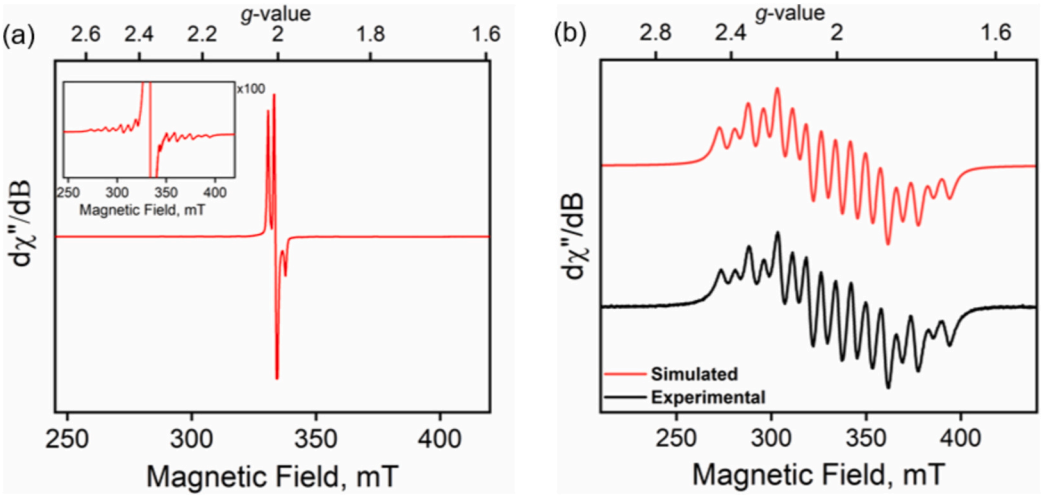

Fig. 4. CW X-band EPR spectra recorded at 13 K (microwave power: 0.016 mW, 5 G modulation amplitude) in a 1:1 MeCN:Toluene solvent mixture for (a) after the reaction of **3**-*cis* with O_2 in the presence of TEMPO-H showing the formation of a TEMPO radical (TEMPO•) (inset: 100× magnified spectrum showing the ^{55}Mn-hyperfine signal of **1**) and (b) isolated **1** (1.0 mM). Anisotropic *g* tensors: $g_{\perp}^{eff} = 2.003$, $g_{\parallel}^{eff} = 2.005$ and hyperfine coupling constant, $|A|$ tensors (MHz):$|A(Mn_A)_{\perp,\parallel}| =$ [439, 204], $|A(Mn_B)_{\perp,\parallel}| =$ [225, 117].

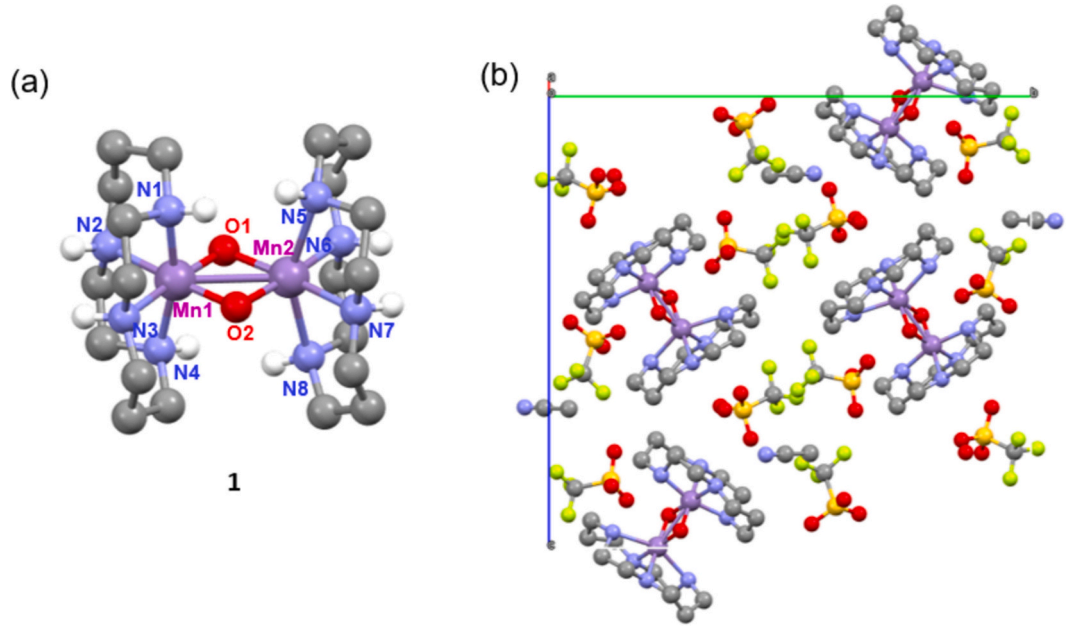

Fig. 5. (a) Single crystal XRD-determined molecular structure of **1.** Hydrogen atoms bonded to atoms other than nitrogen are removed for clarity. Selected bond distances: Mn1-O1 = 1.791 (2) Å, Mn1-O2 = 1.793 (2) Å, Mn2-O1 = 1.856 (2) Å, Mn2-O2 = 1.858 (2) Å and intermetallic separation: Mn1-Mn2 = 2.731 (2) Å. See **Table S4** for crystallographic information. (b) Unit cell packing of the molecules in the crystal. Colour code: C: gray; N: blue; F: green; O: red; S: yellow, Mn: purple. (For interpretation of the references to colour in this figure legend, the reader is referred to the web version of this article.)

structure of **1** (**Fig. S3**). We rather propose an unprecedented trinuclear mechanism of O_2 activation, as shown in Scheme 1, which is also corroborated by the co-crystallization of a Mn(II) center together with the $Mn_2^{IV}O_2$ core in **2** (Scheme 1, Path A). The change of stereochemistry from *cis*-V to *trans*-III for one of the manganese centers can be plausibly attributed to steric requirements for bringing the three Mn centers sufficiently close for O_2 activation. Further support of a trinuclear mechanism comes from kinetic studies associated with the formation of the mixed-valent bis(μ-oxo)$Mn^{III}Mn^{IV}$ complex **1**, upon O_2 activation by **3**-*cis* in presence of TEMPO-H (Scheme 1, Path B). The faster rate of reaction in presence of TEMPO-D relative to TEMPO-H is consistent with the presence of concerted/sequential MnO-OMn cleavage and MnO-H bond formation in the rate-determining steps, where the MnO-D bond in the transition state, an agostic interaction, is more stabilized relative to the MnO-H bond.

CRediT authorship contribution statement

Tarali Devi: Writing – original draft, Investigation, Data curation. **Stefan Mebs:** Writing – review & editing, Investigation, Formal analysis, Data curation. **Dibya Jyoti Barman:** Investigation, Formal analysis, Data curation. **Amanda Opis-Basilio:** Formal analysis. **Michael Haumann:** Writing – review & editing, Investigation, Formal analysis, Data curation, Conceptualization. **Kallol Ray:** Writing – review & editing, Project administration, Investigation, Funding acquisition, Formal analysis, Conceptualization.

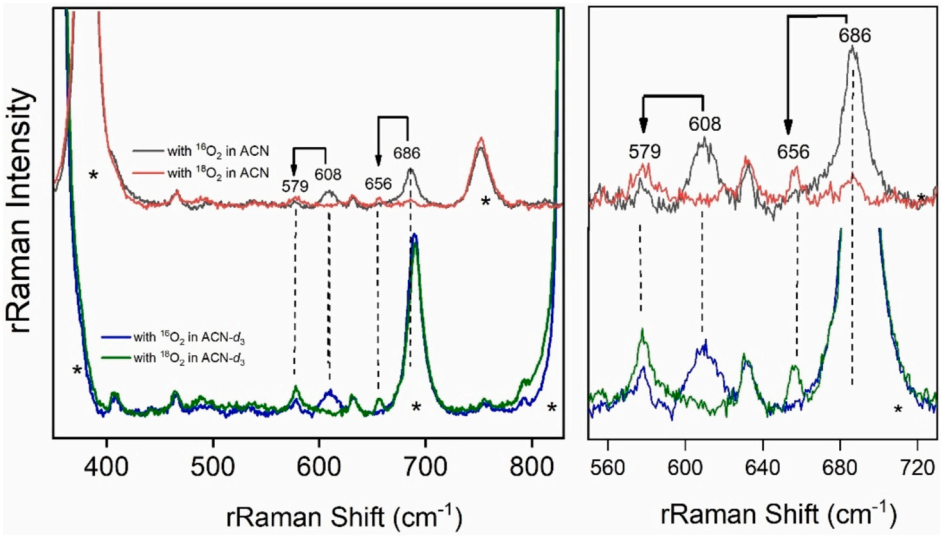

Fig. 6. rRaman spectra (left panel) of **1** (4.0 mM) in ACN (top) and ACN-d_3 (bottom) at −40 °C upon 406 nm laser excitation, (the right panel shows part of the same spectra in magnification). The spectra generated with $^{16}O_2$ and $^{18}O_2$ in ACN are marked in black or red respectively. The spectra generated with $^{16}O_2$ and $^{18}O_2$ in ACN-d_3 are marked in blue or green respectively. Solvent bands are marked with asterisks (*).

Declaration of competing interest

The authors declare that they have no known competing financial interests or personal relationships that could have appeared to influence the work reported in this paper.

Data availability

Data will be made available on request.

Acknowledgements

This work was funded by the Deutsche Forschungsgemeinschaft (DFG, German Research Foundation) under Germany's Excellence Strategy EXC 2008-390540038—UniSysCat and a Heisenberg-Professorship to K.R. A.O.B. thanks Einstein Foundation Berlin (ESB)—Einstein Center of Catalysis (EC^2) for their scholarship and support. T.D. thanks AvH foundation and Grants-in-Aid (CRG/2023/005481) from SERB-DST. We acknowledge the Helmholtz Zentrum Berlin (HZB) for providing experimental infrastructure and allocating beamtime at beamline KMC-3 of the BESSY synchrotron and Dr. I. Zizak and further KMC-3/HZB staff for technical support.

Appendix A. Supplementary data

Supplementary data to this article can be found online at https://doi.org/10.1016/j.jinorgbio.2024.112809.

References

[1] M. Costas, M.P. Mehn, M.P. Jensen, L. Que, Dioxygen activation at mononuclear nonheme iron active sites: enzymes, models, and intermediates, Chem. Rev. 104 (2004) 939–986.
[2] E.G. Kovaleva, M.B. Neibergall, S. Chakrabarty, J.D. Lipscomb, Finding intermediates in the O_2 activation pathways of non-heme iron oxygenases, Acc. Chem. Res. 40 (2007) 475–483.
[3] B.J. Wallar, J.D. Lipscomb, Dioxygen activation by enzymes containing binuclear non-Heme Iron clusters, Chem. Rev. 96 (1996) 2625–2658.
[4] S. Sahu, D.P. Goldberg, Activation of dioxygen by iron and manganese complexes: a heme and nonheme perspective, J. Am. Chem. Soc. 138 (2016) 11410–11428.
[5] J.Y. Lee, K.D. Karlin, Elaboration of copper–oxygen mediated C–H activation chemistry in consideration of future fuel and feedstock generation, Curr. Opin. Chem. Biol. 25 (2015) 184–193.
[6] C.E. Tinberg, S.J. Lippard, Dioxygen activation in soluble methane monooxygenase, Acc. Chem. Res. 44 (2011) 280–288.
[7] I.G. Denisov, T.M. Makris, S.G. Sligar, I. Schlichting, Structure and chemistry of cytochrome P450, Chem. Rev. 105 (2005) 2253–2277.
[8] K. Ray, F.F. Pfaff, B. Wang, W. Nam, Status of reactive non-heme metal-oxygen intermediates in chemical and enzymatic reactions, J. Am. Chem. Soc. 136 (2014) 13942–13958.
[9] E.A. Lewis, W.B. Tolman, Reactivity of Dioxygen−Copper Systems, Chem. Rev. 104 (2004) 1047–1076.
[10] a) D. Kass, T. Corona, K. Warm, B. Braun-Cula, U. Kuhlmann, E. Bill, S. Mebs, M. Swart, H. Dau, M. Haumann, P. Hildebrandt, K. Ray, Stoichiometric formation of an Oxoiron(IV) complex by a soluble methane monooxygenase type activation of O_2 at an Iron(II)-Cyclam center, J. Am. Chem. Soc. 142 (2020) 5924–5928;
b) A. Sen, N.J. Britto, D. Kass, K. Ray, G. Rajaraman, Origin of unprecedented formation and reactivity of Fe^{IV}=O species via oxygen activation: role of noncovalent interactions and magnetic coupling, Inorg. Chem. 63 (2024) 9809–9822.
[11] D.A. Quist, D.E. Diaz, J.J. Liu, K.D. Karlin, Activation of dioxygen by copper metalloproteins and insights from model complexes, J. Biol. Inorg. Chem. 22 (2017) 253–288.
[12] J. Hohenberger, K. Ray, Meyer Karsten, The biology and chemistry of high-valent iron-oxo and iron-nitrido complexes, Nat. Commun. 3 (2012) 720.
[13] K. Ray, F. Heims, M. Schwalbe, High-valent metal-oxo intermediates in energy demanding processes: from dioxygen reduction to water splitting, Curr. Opin. Chem. Biol. 25 (2015) 159–171.
[14] E.G. Kovaleva, J.D. Lipscomb, Science 316 (2007) 453.
[15] J.M. Bollinger Jr., C. Krebs, Curr. Opin. Chem. Biol. 11 (2007) 151.
[16] W.N. Oloo, L. Que Jr., Bioinspired Nonheme Iron Catalysts for C–H and C═C Bond Oxidation: Insights into the Nature of the Metal-Based Oxidants, Acc. Chem. Res. 48 (2015) 2612–2621.
[17] J. Cho, R. Sarangi, W. Nam, Mononuclear metal–O_2 complexes bearing macrocyclic N-Tetramethylated Cyclam ligands, Acc. Chem. Res. 45 (2012) 1321–1330.
[18] a) E.N. Cook, C.W. Machan, Bioinspired mononuclear Mn complexes for O_2 activation and biologically relevant reactions, Dalton Trans. 50 (2021) 16871–16886;
b) C.P. Horwitz, G.C. Dailey, New insights into the reactivity of Mn(II) coordination complexes with dioxygen, Comments Inorg. Chem. 14 (1993) 283–319;
c) M. Osawa, K. Fujisawa, N. Kitajima, Y. Moro-oka, Dimanganese complexes bridged with a (mu-Carboxylato) unit as models for the active site of manganese catalase (X = OH, O or $(O)_2$), Chem. Lett. 26 (1997) 919–920;
d) C.-M. Lee, W.-Y. Wu, M.-H. Chiang, D.S. Bohle, G.-H. Lee, Generation of a Mn (IV)-Peroxo or Mn(III)-Oxo-Mn(III) species upon oxygenation of mono-and binuclear thiolate-ligated Mn(II) complexes, Inorg. Chem. 56 (2017) 10559–10569;
e) J.D. Parham, G.B. Wijeratne, J.R. Mayfield, T.A. Jackson, Steric control of dioxygen activation pathways for Mn^{II} complexes supported by pentadentate, amide-containing ligands, Dalton Trans. 48 (2019) 13034–13045.
[19] M.K. Coggins, X. Sun, Y. Kwak, E.I. Solomon, E. Rybak-Akimova, J. Kovacs, A. Characterization of metastable intermediates formed in the reaction between a Mn(II) complex and dioxygen, including a crystallographic structure of a binuclear Mn(III)-Peroxo, J. Am. Chem. Soc. 135 (2013) 5631–5640.
[20] R.L. Shook, W.A. Gunderson, J.Z. Greaves, W. Joseph, M.P. Hendrich, A.S. Borovik, A monomeric Mn^{III}-Peroxo complex derived directly from dioxygen, J. Am. Chem. Soc. 130 (2008) 8888–8889.

[21] J.A. Kovacs, Tuning the relative stability and reactivity of manganese dioxygen and Peroxo intermediates via systematic ligand modification, Acc. Chem. Res. 48 (2015) 2744–2753.
[22] M. Guo, Y.M. Lee, R. Gupta, M.S. Seo, T. Ohta, H.H. Wang, H.Y. Liu, S.N. Dhuri, R. Sarangi, S. Fukuzumi, W. Nam, Dioxygen Activation and O–O Bond Formation Reactions by Manganese Corroles, J. Am. Chem. Soc. 139 (2017) 15858–15867.
[23] a) F.L. Domenick, S. Chattopadhyay, V.W. Day, T.A. Jackson, Reaction landscape of a pentadentate N5-ligated Mn^{II}complex with $O_2^{\bullet-}$and H_2O_2 includes conversion of a peroxomanganese(iii) adduct to a bis(μ-oxo)dimanganese(iii,iv) species, Dalton Trans. 42 (2013) 13014–13025;
b) M.U. Triller, W.Y. Hsieh, V.L. Pecoraro, A. Rompel, B. Krebs, Preparation of highly efficient manganese catalase mimics, Inorg. Chem. 41 (2002) 5544–5554;
c) M. Sankaralingam, S.H. Jeon, Y.M. Lee, M.S. Seo, K. Ohkubo, S. Fukuzumi, W. Nam, An amphoteric reactivity of a mixed-valent bis(μ-oxo)dimanganese(iii,iv) complex acting as an electrophile and a nucleophile, Dalton Trans. 45 (2016) 376–383.
[24] S. Hong, Y.M. Lee, M. Sankaralingam, A.K. Vardhaman, Y.J. Park, K.B. Cho, T. Ogura, R. Sarangi, S. Fukuzumi, W. Nam, A manganese(V)–Oxo complex: synthesis by dioxygen activation and enhancement of its oxidizing power by binding scandium ion, J. Am. Chem. Soc. 138 (2016) 8523–8532.
[25] D. Brazzolotto, F.G. Cantú Reinhard, J. Smith-Jones, M. Retegan, L. Amidani, A. S. Faponle, K. Ray, C. Philouze, S.P. Visser, M. Gennari, C. Duboc, A high-valent non-heme μ-oxo manganese(IV) dimer generated from a thiolate-bound manganese (II) complex and dioxygen, Angew. Chem. Int. Ed. 56 (2017) 8211–8215.
[26] J.A. Cotruvo, T.A. Stich, R.D. Britt, J. Stubbe, Mechanism of assembly of the dimanganese-tyrosyl radical cofactor of class Ib ribonucleotide reductase: enzymatic generation of superoxide is required for tyrosine oxidation via a Mn(III) Mn(IV) intermediate, J. Am. Chem. Soc. 135 (2024) 4027–4039.
[27] B. Battistella, T. Lohmiller, B. Cula, P. Hildebrandt, U. Kuhlmann, H. Dau, S. Mebs, K. Ray, A new thiolate-bound Dimanganese cluster as a structural and functional model for class Ib ribonucleotide reductases, Angew. Chem. Int. Ed. 62 (2023) e202217076.
[28] K.J. Brewer, M. Calvin, R.S. Lumpkin, J.W. Otvos, L. Spreer, Synthesis, structure, and characterization of a mixed-valence manganese(III)-manganese(IV)-Bis(μ-oxo) complex with a macrocyclic tetraaza ligand, Inorg. Chem. 28 (1989) 4446–4451.
[29] K.J. Brewer, A. Liegeois, J.W. Otvos, M. CaIvin, L. Spreer, Synthesis and properties of two bimetallic mixed-valence Di-μ-oxo manganese complexes with different tetraaza macrocyclic ligands, J. Chem. Soc. Chem. Commun (1988) 1219–1220.
[30] a) T. Hunter, I. McNae, X. Liang, J. Bella, S. Parsons, M. Walkinshaw, P. Sadler, Protein recognition of macrocycles: binding of anti-HIV metallocyclams to lysozyme, Proc. Natl. Acad. Sci. U. S. A. 102 (2005) 2288–2292.b)The quality of the structure is not good enough, but nevertheless it confirms the bond connectivity and the *cis* configuration.
[31] H. Nakamori, T. Matsumoto, T. Yatabe, K.S. Yoon, H. Nakaiab, S. Ogo, Synthesis and crystal structure of a dinuclear, monomeric Mn^{II} p-semiquinonato complex, Chem. Commun. 50 (2014) 13059–13061.
[32] M.K. Coggins, A.N. Downing, W. Kaminsky, J.A. Kovacs, Comparison of two $Mn^{IV}Mn^{IV}$-bis-μ-oxo complexes $\{[Mn^{IV}(N_4(6\text{-Me-DPEN}))]_2(\mu\text{-}O)_2\}^{2+}$ and $\{[Mn^{IV}(N_4(6\text{-Me-DPPN}))]_2(\mu\text{-}O)_2\}^{2+}$, Acta Crystallogr. E76 (2020) 1042–1046.
[33] P.A. Goodson, Glerup Jorgen, D.J. Hodgson, K. Michelsen, Pedersen Erik, Binuclear Bis(μ-oxo)dimanganese (III, IV) and-(IV,IV) Complexes with N, N'-Bis(2-pyridylmethyl)-1,2-ethanediamine, Inorg. Chem. 29 (1990) 503–508.
[34] S. Mukhopadhyay, S.K. Mandal, S. Bhaduri, W.H. Armstrong, Manganese clusters with relevance to photosystem II, Chem. Rev. 104 (2004) 3981–4026.
[35] B.C. Dave, R.S. Czernuszewicz, One-equivalent oxidative charge storage on an $[Mn_2O_2]^{3+}$ core: synthesis, crystal structure and resonance Raman spectra of $[Mn_2O_2(pbz)_4]^{n+}$ (n = 3, 4), Inorg Chim Act 227 (1994) 33–41.
[36] X. Lu, X.X. Li, M.S. Seo, Y.M. Lee, M. Clémancey, P. Maldivi, J.M. Latour, R. Sarangi, S. Fukuzumi, W. Nam, A mononuclear Nonheme Iron(IV)−Amido complex relevant for the compound II chemistry of cytochrome P450, J. Am. Chem. Soc. 141 (2019) 80–83.
[37] W.D. Jones, Isotope effects in C-H BondActivation reactions by transition metals, Acc. Chem. Res. 36 (2003) 140–146.
[38] P.L. Fernandez, A.S. Murkin, Inverse solvent isotope effects in enzyme-catalyzed reactions, Molecules 25 (2020) 1933.
[39] H. Johnston, D.M. Freire, C. Mantsorov, Jamison Nena, K.N. Green, Manganese(III/IV)μ-Oxo dimers and manganese(III) monomers with tetra aza macrocyclic ligands and historically relevant open-chain ligands. Eur, J. Inorg. Chem. (2022) 1–19, e202200039.
[40] H.A. Chu, W. Hillier, N.A. Law, G.T. Babcock, Vibrational spectroscopy of the oxygen-evolving complex and of manganese model compounds, Biochim. Biophys. Acta 1503 (2001) 69–82.
[41] H. Dau, P. Liebisch, M. Haumann, X-ray absorption spectroscopy to analyze nuclear geometry and electronic structure of biological metal centers—potential and questions examined with special focus on the tetra-nuclear manganese complex of oxygenic photosynthesis, Anal. Bioanal. Chem. 376 (2003) 562–583.
[42] X. Engelmann, D.D. Malik, T. Corona, K. Warm, E.R. Farquhar, M. Swart, W. Nam, K. Ray, Trapping of a highly reactive oxoiron(IV) complex in the catalytic epoxidation of olefins by hydrogen peroxide, Angew. Chem. Int. Ed. 58 (2019) 4012–4016.